Article

Neuron

Hippocampal-Prefrontal Theta Transmission Regulates Avoidance Behavior

Highlights

- Oscillatory, not pulsatile, stimulation of vHPC-mPFC at 8 Hz increased avoidance
- Oscillatory stimulation of vHPC-mPFC at 2 or 20 Hz did not increase avoidance
- Oscillatory stimulation of vHPC-mPFC facilitated neural transmission in this pathway
- 8-Hz oscillatory stimulation increased vHPC-mPFC theta synchrony during the EPM

Authors

Nancy Padilla-Coreano, Sarah Canetta, Rachel M. Mikofsky, ..., Christoph Kellendonk, David A. Kupferschmidt, Joshua A. Gordon

Correspondence

joshua.gordon@nih.gov

In Brief

Padilla-Coreano et al. investigated the role of vHPC-mPFC theta synchrony in avoidance behavior. They demonstrate that, compared to other frequencies, oscillatory optogenetic stimulation of vHPC terminals in mPFC at 8 Hz maximally increases avoidance, enhances neural transmission, and increases synchrony in this pathway.

Padilla-Coreano et al., 2019, Neuron *104*, 601–610
November 6, 2019 Published by Elsevier Inc.
https://doi.org/10.1016/j.neuron.2019.08.006

CellPress

Neuron
Article

Hippocampal-Prefrontal Theta Transmission Regulates Avoidance Behavior

Nancy Padilla-Coreano,[1,8] Sarah Canetta,[2,4,8] Rachel M. Mikofsky,[5] Emily Alway,[5] Johannes Passecker,[5,7] Maxym V. Myroshnychenko,[5] Alvaro L. Garcia-Garcia,[2] Richard Warren,[2] Eric Teboul,[4] Dakota R. Blackman,[2] Mitchell P. Morton,[2] Sofiya Hupalo,[5] Kay M. Tye,[1] Christoph Kellendonk,[2,3,4] David A. Kupferschmidt,[5] and Joshua A. Gordon[5,6,9,*]

[1]Systems Neuroscience Laboratory, The Salk Institute for Biological Studies, La Jolla, CA 92037, USA
[2]Department of Psychiatry, Columbia University Medical Center, 1051 Riverside Drive, New York, NY 10032, USA
[3]Department of Pharmacology, Columbia University Medical Center, 1051 Riverside Drive, New York, NY 10032, USA
[4]Division of Molecular Therapeutics, New York State Psychiatric Institute, New York, NY 10032, USA
[5]Integrative Neuroscience Section, National Institute of Neurological Disorders and Stroke, NIH, Bethesda, MD 20892, USA
[6]National Institute of Mental Health, NIH, Bethesda, MD 20892, USA
[7]Zuckerman Mind Brain Behavior Institute, New York, NY 10027, USA
[8]These authors contributed equally
[9]Lead Contact
*Correspondence: joshua.gordon@nih.gov
https://doi.org/10.1016/j.neuron.2019.08.006

SUMMARY

Long-range synchronization of neural oscillations correlates with distinct behaviors, yet its causal role remains unproven. In mice, tests of avoidance behavior evoke increases in theta-frequency (~8 Hz) oscillatory synchrony between the ventral hippocampus (vHPC) and medial prefrontal cortex (mPFC). To test the causal role of this synchrony, we dynamically modulated vHPC-mPFC terminal activity using optogenetic stimulation. Oscillatory stimulation at 8 Hz maximally increased avoidance behavior compared to 2, 4, and 20 Hz. Moreover, avoidance behavior was selectively increased when 8-Hz stimulation was delivered in an oscillatory, but not pulsatile, manner. Furthermore, 8-Hz oscillatory stimulation enhanced vHPC-mPFC neurotransmission and entrained neural activity in the vHPC-mPFC network, resulting in increased synchrony between vHPC theta activity and mPFC spiking. These data suggest a privileged role for vHPC-mPFC theta-frequency communication in generating avoidance behavior and provide direct evidence that synchronized oscillations play a role in facilitating neural transmission and behavior.

INTRODUCTION

Neural oscillations—rhythmic fluctuations of neural activity—have been observed in many brain regions and correlate with behavioral states in a variety of mammals, including humans (Buzsáki and Watson, 2012; Buzsáki et al., 2012; Harris and Gordon, 2015). Frequency-specific synchronization of these oscillations between regions has also been linked to behavior (Harris and Gordon, 2015), providing a potential translatable substrate for understanding changes in functional connectivity associated with specific behaviors and disease states (Uhlhaas and Singer, 2012). However, evidence linking long-range oscillatory synchronization to alterations in neural transmission and behavior remains largely correlational and therefore speculative. To address this issue, we turned to a rodent paradigm—the elevated plus maze (EPM)—wherein synchrony between the ventral hippocampus (vHPC) and medial prefrontal cortex (mPFC) within the theta-frequency range (4–12 Hz) has been extensively correlated to avoidance of the open arms (Adhikari et al., 2011; Likhtik et al., 2014; Padilla-Coreano et al., 2016). Exposure to anxiogenic environments enhances vHPC-mPFC theta synchrony. This enhancement is reflected by synchronization of local field potentials (LFPs) in the two regions, as well as by entrainment of spiking of mPFC neurons to theta oscillations in the vHPC LFP (Adhikari et al., 2010). Moreover, theta activity in the vHPC-mPFC circuit is linked to the construction of neural representations of aversion within the mPFC (Adhikari et al., 2011; Padilla-Coreano et al., 2016). Optogenetic inhibition of the direct projection from the vHPC to the mPFC ablates these representations and reduces both theta-frequency synchrony and avoidance behavior (Kjaerby et al., 2016; Padilla-Coreano et al., 2016). Furthermore, a recent study showed that chemogenetic activation of mPFC-projecting vHPC cells increases avoidance behavior (Parfitt et al., 2017). However, these findings leave open the question as to whether increased theta-frequency oscillatory synchrony plays a causal role in generating avoidance behavior and in facilitating vHPC-mPFC communication or is merely a byproduct of that communication.

RESULTS

Oscillatory Stimulation of vHPC-mPFC at 8 Hz Is Sufficient to Increase Avoidance Behavior

To address this question, we attempted to optogenetically mimic the naturally occurring oscillations in the vHPC-mPFC

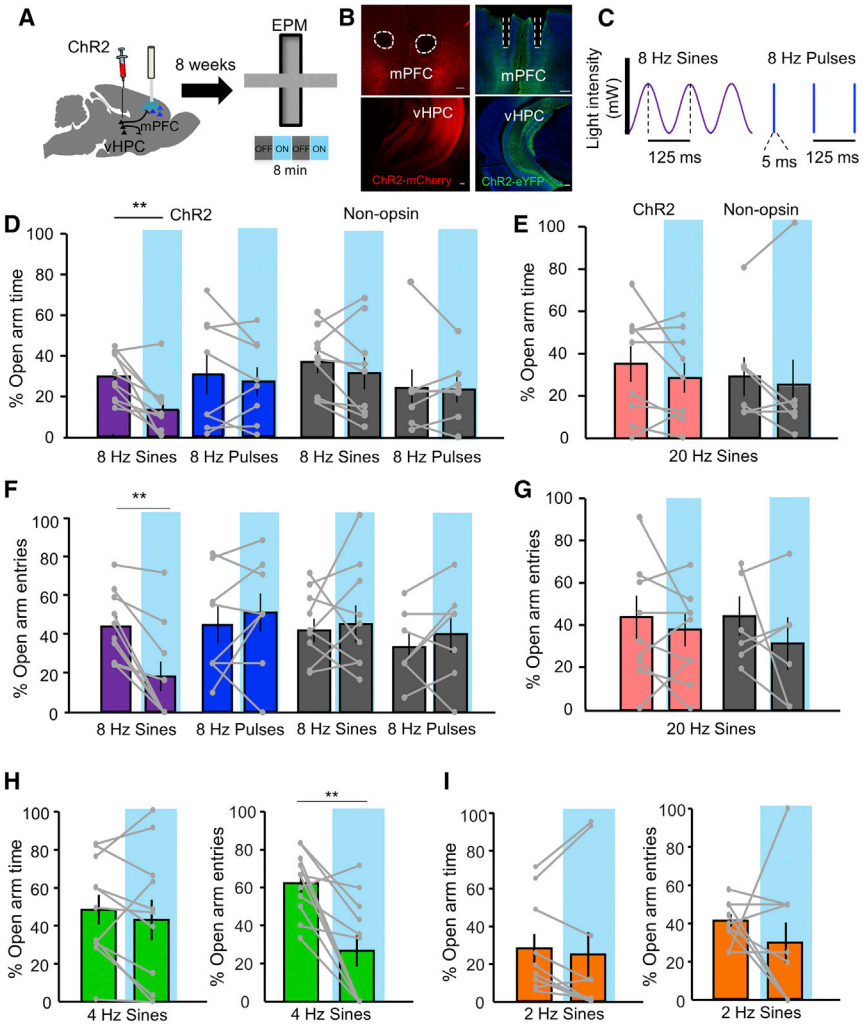

Figure 1. Theta-Frequency Oscillatory Stimulation of vHPC-mPFC Inputs Increases Avoidance Behavior

(A) Experimental schematic. Adeno-associated virus (AAV) encoding ChR2 or a non-opsin fluorophore was injected into the vHPC, and optical stimulation fibers were implanted over the mPFC. 8 weeks later, patterned light stimulation was delivered to vHPC terminals in the mPFC during exploration of the elevated plus maze (EPM) in 2-min epochs.

(B) Example of CaMKIIa-ChR2(H134)-mCherry (left) and CaMKIIa-ChR2(H134)-eYFP (right; blue: neurotrace) viral expression and positioning of optical fibers (dashed lines) in the mPFC (top) and in vHPC (bottom). Scale bars, 100 μm (left) and 200 μm (right).

(C) Light was delivered to the mPFC in oscillatory versus pulsatile patterns at 8 Hz.

(D) % Open arm time in the EPM as a function of light pattern and virus type for 8-Hz stimulation (ChR2: 8-Hz sines n = 10, 8-Hz pulses n = 9; non-opsin control: 8-Hz sines n = 9, 8-Hz pulses n = 7; only 8-Hz sines group meets Bonferroni-corrected significance with a paired comparison; paired t test for 8 Hz **p = 0.0032). Blue background indicates light ON epochs, and error bars indicate SEM.

(E) % Open time as a function of virus type for 20-Hz oscillatory stimulation (ChR2, n = 9; non-opsin, n = 6; two-way rmANOVA, no main effect of light, $F_{(1,13)}$ = 1.854, p = 0.1964; Bonferroni post hoc, ChR2 20 Hz sines ON versus OFF, multiplicity-adjusted p = 0.4797).

(F) % Entries into open arms as a function of light pattern and virus type for 8-Hz stimulation (ChR2: 8 Hz sines, n = 10; 8 Hz pulses, n = 9; non-opsin: 8 Hz sines, n = 9; 8 Hz pulses, n = 7; only 8-Hz sines group meets Bonferroni-corrected significance with a paired comparison; paired t test for 8 Hz **p = 0.0008).

(G) % Entries into open arms as a function of light pattern and virus type for 20-Hz stimulation (ChR2: n = 9; non-opsin n = 6; two-way rmANOVA no effect of light $F_{(1,13)}$ = 1.66, p = 0.22 or interaction between virus and light $F_{(1,13)}$ = 0.2345, p = 0.63).

(H) % Open arm time (left) and % open arm entries (right) in the EPM for 4-Hz oscillatory stimulation in ChR2-expressing mice (n = 10; % open arm time: paired t test p = 0.4162; % open arm entries: paired t test **p = 0.0032).

(I) % Open arm time (left) and % open arm entries (right) in the EPM for 2-Hz oscillatory stimulation in ChR2-expressing mice (n = 10 mice; % open arm time: paired t test p = 0.5521; % open arm entries: paired t test p = 0.3527).

See also Figures S1 and S2.

circuit by using a theta-frequency (8 Hz) light pattern to activate ChR2-expressing vHPC terminals in the mPFC of mice. Light was delivered in a continuous oscillatory sinusoidal pattern, or in a pulsatile pattern with 5-ms pulses. Adeno-associated viruses encoding CaMKIIa promoter-driven ChR2(H134)-mCherry or non-opsin control constructs were injected bilaterally into the vHPC of wild-type 129SvevTac mice, and bilateral optical fibers were implanted in the mPFC for localized terminal stimulation (Figures 1A–1C). Patterned illumination was alternated with no illumination for 2-min epochs in the EPM with either oscillatory or pulsatile light (Figure 1A). Oscillatory, but not pulsatile, stimulation at 8 Hz in ChR2-expressing mice increased avoidance of the open arms (Figures 1D and 1F). Importantly, these effects were specific to 8-Hz stimulation frequency, as oscillatory stimulation delivered at 20 Hz did not affect open arm avoidance (Figures 1E and 1G).

To rule out the possibility that 8-Hz oscillatory stimulation was simply enhancing preference for the animal's current environment, we assessed the effects of this stimulation paradigm stratified by the arm the animal was in at the time stimulation occurred. The effect of 8-Hz oscillatory stimulation in the EPM was the same regardless of which maze compartment mice were exploring at light onset (Figure S1A). These findings support the conclusion that 8-Hz oscillatory stimulation induces avoidance behavior rather than increasing preference for or against a current location. Importantly, locomotion in the EPM was not affected by oscillatory stimulation

at 8 Hz or 20 Hz or by 8-Hz pulsatile terminal stimulation (Figure S1B).

To further determine whether theta-frequency activation of the vHPC-mPFC circuit exerts a privileged influence on avoidance behavior or whether its effects could be reproduced by lower frequency oscillatory stimulation, we tested the effects of 4-Hz and 2-Hz oscillatory stimulation on avoidance behavior. Oscillatory stimulation at 4 Hz revealed inconsistent effects on measures of avoidance, with a significant reduction in % open arm entries, but not % open arm time (Figure 1H). Locomotion during the 4-Hz stimulation decreased over time across the light epochs (Figure S2A), an effect that was not seen during 8-Hz oscillatory stimulation (data not shown; two-way rmANOVA no significant main effects of light, epoch, or their interaction). No effect of 4-Hz oscillatory stimulation was seen on % open arm time, regardless of which maze compartment mice were exploring at light onset (Figure S2B). Retesting this cohort of mice on the EPM 3 weeks later with 2-Hz oscillatory stimulation revealed that 2-Hz stimulation had no effect on avoidance behavior but decreased locomotion (Figures 1H and S2C). Mice that were in an open arm at 2-Hz light onset also showed greater % open arm time relative to mice in other compartments at light onset (Figure S2D). Altogether, these data suggest that there is an optimal frequency range for oscillatory stimulation of vHPC-mPFC to induce avoidance behavior.

Oscillatory Optogenetic Stimulation of vHPC Terminals Results in Increased Spontaneous-like Excitatory Neurotransmission in mPFC

To understand how pulsatile and oscillatory optogenetic terminal stimulations differ in their effects on the vHPC-mPFC pathway, we examined the effects of our optogenetic stimulation paradigms on vHPC-mPFC neural transmission in acute brain slices *ex vivo*. Whole-cell patch-clamp recordings of layer 3 and 5 mPFC pyramidal cells were performed while stimulating ChR2-expressing vHPC terminals with pulsatile or oscillatory light. mPFC pyramidal cells were voltage-clamped at −70 mV. vHPC terminals surrounding the patched cells were illuminated via an optical fiber, and excitatory postsynaptic currents (EPSCs) were quantified before and during light stimulation (Figures 2A–2C). All stimulation patterns significantly increased EPSC frequency relative to the pre-stimulation baseline (Figure 2C, top panel). Importantly, the frequency of EPSCs evoked during light stimulation remained consistent over the light duration (Figure 2D). However, the EPSCs evoked by pulsatile and oscillatory stimulation differed in nature. Pulsatile stimulation evoked large-amplitude EPSCs time locked to each optical pulse (Figures 2B and 2C). Oscillatory stimulation, by contrast, did not induce stimulus-locked, large-amplitude EPSCs but rather increased the rate of spontaneous-like EPSCs that were similar in amplitude to those seen during the pre-stimulation baseline (Figures 2B and 2C). Unlike pulse-induced EPSCs, these oscillation-induced EPSCs were not phase locked to the oscillatory stimulus (Figures 2E–2G). Together, these data suggest that oscillatory stimulation increases excitatory transmission in the mPFC, perhaps via subthreshold depolarizations that increase release probability at vHPC terminals.

8-Hz Oscillatory, but Not Pulsatile, Optogenetic Stimulation Facilitates Evoked vHPC-mPFC Neurotransmission

We hypothesized that the subtle increases in mPFC excitatory transmission observed in response to 8-Hz oscillatory stimulation of the vHPC-mPFC pathway *ex vivo* would facilitate ongoing vHPC-mPFC neurotransmission *in vivo*. To test this hypothesis, we investigated the ability of optical stimulation to enhance electrically evoked vHPC-mPFC transmission in anesthetized mice. Mice injected with ChR2 in the vHPC were anesthetized with isoflurane. A tungsten stimulating electrode inserted into the vHPC was used to stimulate vHPC somas (100-μs pulses of 200–400 μA delivered pseudorandomly) while an optrode in the mPFC delivered light and recorded extracellular spiking (Figures 3A and 3B). Electrical stimulation of the vHPC generated postsynaptic spiking responses in the mPFC with a characteristic onset latency of 10 ms (Figures 3C and 3D), consistent with reported monosynaptic latencies for this pathway (Spellman et al., 2015; Tierney et al., 2008). Optical activation of ChR2-containing vHPC terminals in the mPFC was superimposed onto the ongoing, pseudorandom vHPC electrical activation, resulting in vHPC stimulation at varying phases of the optical stimulation (Figures S3A and S3B). Superimposing either 8-Hz or 20-Hz oscillatory light onto vHPC terminals increased the peak evoked firing rate of mPFC single units in response to vHPC electrical stimulation, whereas 8-Hz pulsatile stimulation had no such effect (Figures 3D and S3C). The effect of oscillatory stimulation was highly dependent on the phase of stimulation, with the maximum enhancement of evoked firing occurring in the falling phase (Figures 3E, S3E, and S3F). Consistent with a privileged role for theta frequencies in this pathway, oscillatory stimulation at 8 Hz increased evoked firing rate during this falling phase to a significantly greater extent than 20-Hz oscillatory stimulation (Figure 3F). Given the short duration of the optical pulsatile stimulation (5 ms), we analyzed evoked firing at time points closer to the peak of the optical pulse. When pulses occurred within milliseconds of the electrical stimulation, responses to vHPC stimulation were mixed; firing was modestly suppressed in 30% of units and modestly increased in 50% of units, resulting in no net effect on firing rate (Figure S3D). These data demonstrate that oscillatory stimulation of vHPC terminals is capable of enhancing vHPC-mPFC neurotransmission in a frequency- and phase-specific manner.

8-Hz Oscillatory Optogenetic Stimulation Synchronizes mPFC and vHPC Neural Activity during Behavior

To examine whether the facilitatory effects of 8-Hz oscillatory stimulation also occurred in behaving animals, mice expressing ChR2 or a non-opsin fluorophore in vHPC neurons were implanted with optrodes in the mPFC. Single units were recorded during vHPC terminal illumination at either 8 or 20 Hz at baseline (during exploration of a familiar environment) and while exploring the EPM. Oscillatory stimulation at either frequency in either environment had no effect on the overall firing rate of mPFC cells (Figure 4). We next examined whether the optical stimuli entrained mPFC spiking *in vivo* by calculating the phase locking of mPFC spikes to the optical stimulus (Vinck et al., 2010). At baseline, both oscillatory stimuli induced phase locking of mPFC spiking to the optical stimulus to the same degree (Figures 5A and 5B).

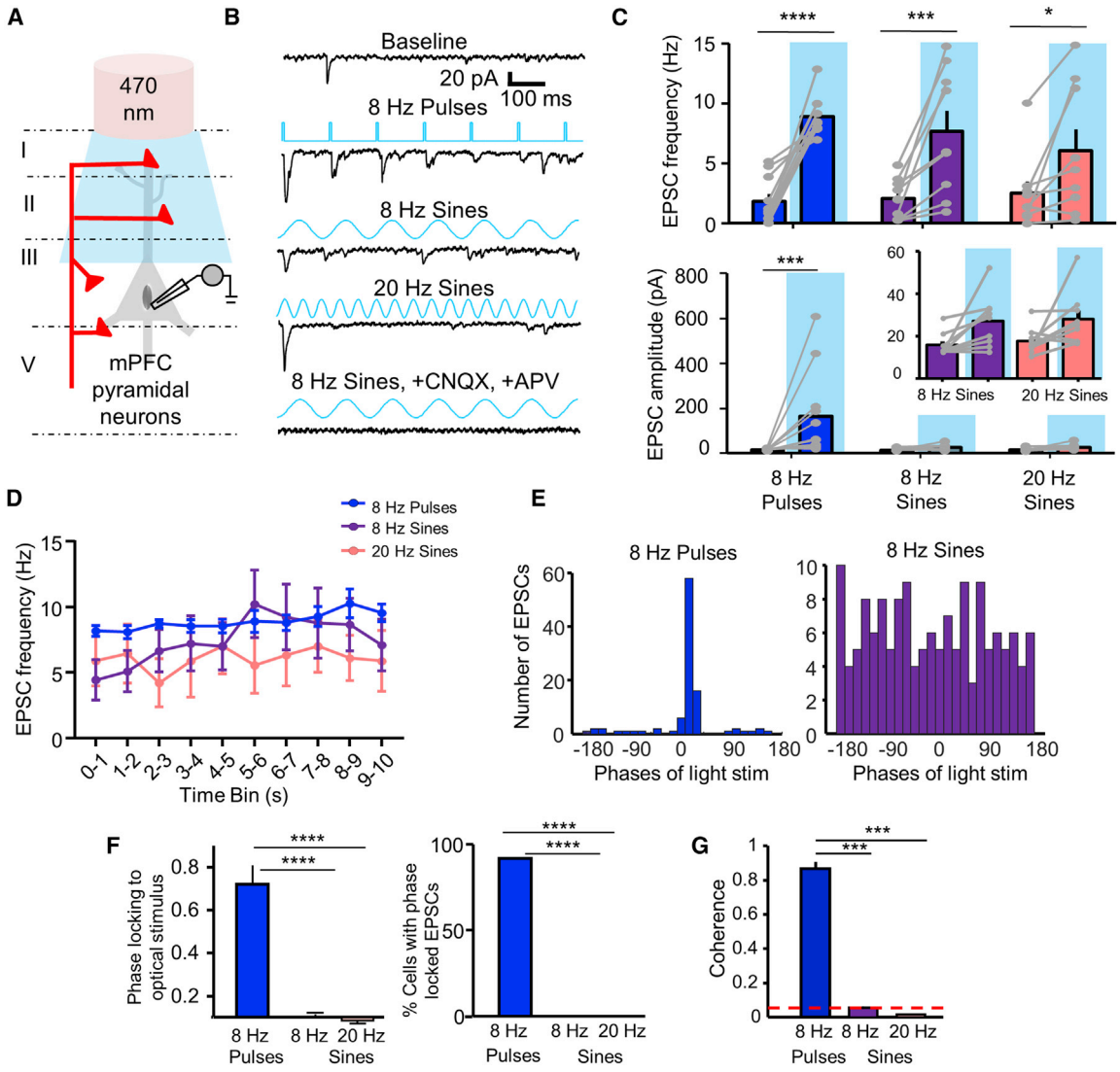

Figure 2. Oscillatory Stimulation of ChR2-Expressing vHPC Terminals in the mPFC Enhances Spontaneous-like Activity in an *Ex Vivo* Slice Preparation

(A) Experimental schematic. Voltage clamp recordings were obtained from mPFC pyramidal cells held at −70 mV while an optical fiber stimulated vHPC ChR2-containing terminals *ex vivo*.

(B) Representative excitatory postsynaptic current (EPSC) responses to the various stimulation patterns. Bottom trace shows postsynaptic current during oscillatory stimulation following application of the glutamate receptor blockers CNQX and APV.

(C) Average EPSC frequency (top) and amplitude (bottom) at baseline versus during light stimulation (8-Hz pulses n = 11 cells; 8-Hz sines n = 9 cells; 20-Hz sines n = 9 cells; two-way rmANOVA, main effect of light $F_{(1,26)} = 57.24$, $p < 0.0001$; Bonferroni post hoc, 8-Hz pulses ON versus OFF, ****multiplicity-adjusted $p < 0.0001$, 8-Hz sines ON versus OFF, ***multiplicity-adjusted $p = 0.0005$, 20-Hz sines ON versus OFF, *multiplicity-adjusted $p = 0.02597$). (Bottom) Average EPSC amplitude at baseline versus during light stimulation is shown (8-Hz pulses n = 11 cells; 8-Hz sines n = 9 cells; 20-Hz sines n = 9 cells; two-way rmANOVA, light by stimulation interaction, $F_{(2,26)} = 4.572$, *$p = 0.0199$; Bonferroni post hoc, 8-Hz pulses ON versus OFF, ***multiplicity-adjusted $p = 0.0010$).

(D) Average frequency of EPSCs across the duration of the light stimulation (two-way rmANOVA no main effect of time $F_{(9,234)} = 1.89$; $p = 0.0537$).

(E) Representative phase locking of EPSCs to the pulsatile 8-Hz light versus oscillatory 8-Hz light.

(F) (Left) Phase locking of EPSCs to the various optical stimulation patterns as measured by pairwise phase consistency (8-Hz pulses n = 11 cells; 8-Hz sines n = 9 cells; 20-Hz sines n = 9 cells; Wilcoxon rank-sum 8-Hz pulses versus 8-Hz sines ****$p = 0.00048$; Wilcoxon rank-sum 8-Hz pulses versus 20-Hz sines ****$p = 0.00052$). (Right) % cells with EPSCs that are significantly phase locked to the different optical stimulation patterns (chi-square 8-Hz pulses versus 8-Hz sines ****$p < 0.0001$; chi-square 8-Hz pulses versus 20-Hz sines ****$p < 0.0001$).

(G) Coherence between the continuous amplitude of the current trace and the different optical stimulation patterns (rank-sum 8-Hz pulses versus 8-Hz sines, ***$p = 0.00019$; rank-sum 8-Hz pulses versus 20-Hz sines, ***$p = 0.00019$). Red dashed line indicates chance coherence levels obtained from shuffled data. All error bars indicate SEM.

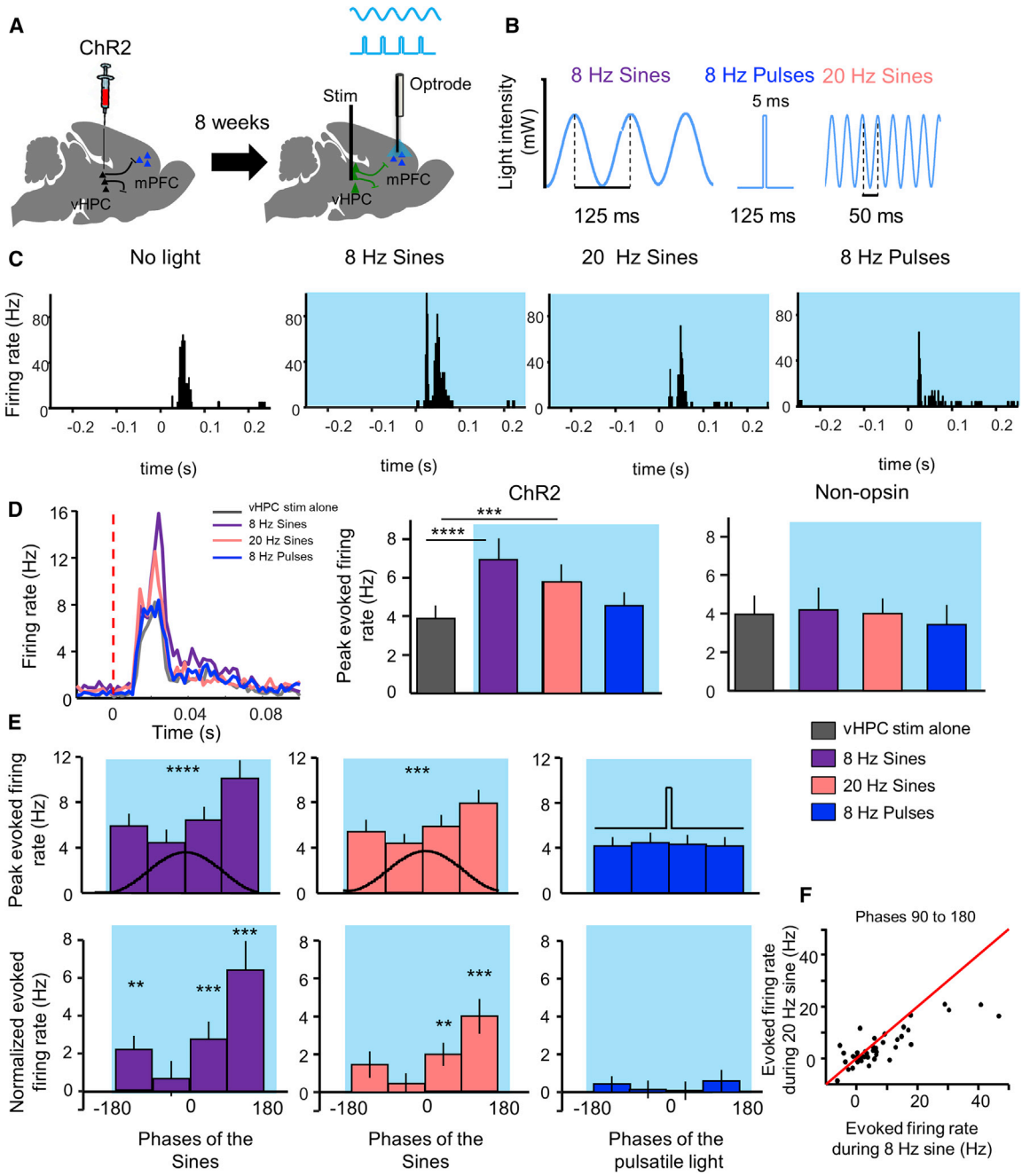

Figure 3. Oscillatory Stimulation of vHPC Terminals at a Theta Frequency Facilitates Ongoing vHPC Input to mPFC *In Vivo*

(A) Experimental schematic. In vHPC ChR2-expressing mice, a stimulating electrode was implanted in the vHPC and an optrode in the ipsilateral mPFC. Electrical stimulation to vHPC (200–400 μA square wave pulse; 0.1 ms) was delivered during patterned optical stimulation of the terminals in the mPFC.

(B) Representation of the light patterns used to optically stimulate vHPC terminals. Note that the peak light power across stimuli was the same.

(C) Example mPFC single unit showing strong evoked responses to vHPC electric stimulation with and without patterned optical stimulation in the mPFC.

(D) (Left) Averaged mPFC single-unit responses to vHPC electrical stimulation as a function of optical stimulation. (Right) Average peak evoked response (10–40 ms post-electrical stimulation) of all mPFC single units recorded from ChR2 mice (n = 50 single units; non-parametric one-way rmFriedman test across groups ****$p < 0.0001$; Dunn's post hoc, 8-Hz sines versus stim alone, ****multiplicity-adjusted $p < 0.0001$, 20-Hz sines versus stim alone, ***multiplicity-adjusted $p = 0.0005$, 8-Hz pulses versus stim alone, multiplicity-adjusted $p = 0.1208$) or single units recorded from non-opsin fluorophore mice (n = 34 single units; non-parametric one-way rmFriedman test across groups $p = 0.5112$).

(E) (Top) Peak evoked firing rates in mPFC across phases of light stimulation (8-Hz sines rmFriedman test across phases ****$p < 0.0001$; 20-Hz sines rmFriedman test ***$p = 0.0002$). Black overlay of light stimulus indicates the phase information. (Bottom) Normalized evoked firing across phases of the light stimulation is

(legend continued on next page)

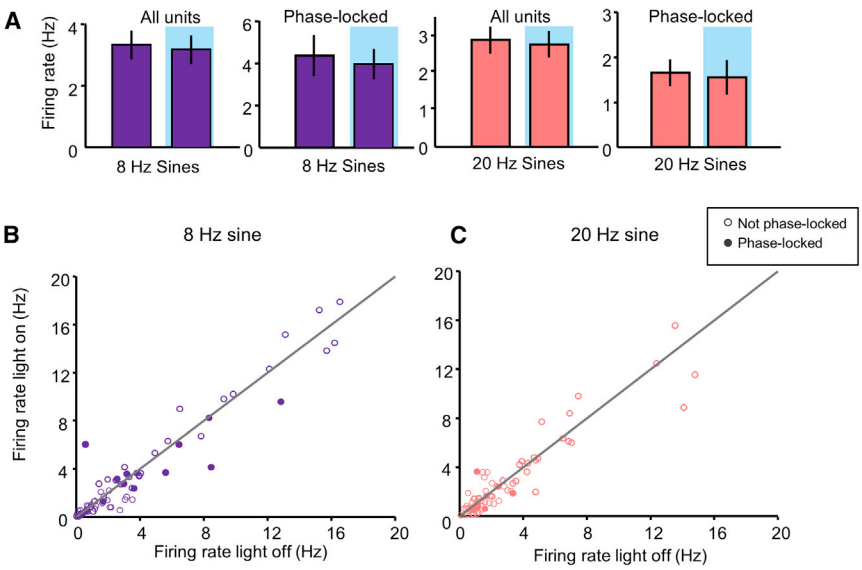

Figure 4. Oscillatory Stimulation of vHPC Terminals Does Not Increase Overall mPFC Firing Rate

(A) Average firing rate with and without 8-Hz and 20-Hz oscillatory stimulation during the EPM for all recorded mPFC single units and of units that were significantly phase-locked to the oscillatory stimulus (8 Hz n = 66, Wilcoxon signed-rank test p = 0.08; 20 Hz n = 67, Wilcoxon signed-rank test p = 0.15) and for significantly phase-locked units (8 Hz n = 14, Wilcoxon signed-rank test p = 0.19; 20 Hz n = 8, Wilcoxon signed-rank test p = 0.25).

(B) Scatterplot showing firing rate of single units stimulated with 8-Hz sines during the EPM (not phase-locked units n = 52, Wilcoxon signed-rank test p = 0.08; phase-locked units n = 14, Wilcoxon signed-rank test p = 0.19).

(C) Scatterplot showing firing rate of single units stimulated with 20-Hz sines during the EPM (not phase-locked units n = 59, Wilcoxon signed-rank test p = 0.15; phase-locked units n = 8, Wilcoxon signed-rank test p = 0.25). Open circles represent non-phase-locked units, and closed circles are units significantly phase locked to the oscillatory stimulus. Error bars indicate SEM.

In contrast, during exposure to the EPM, 8-Hz illumination induced stronger phase locking to the optical stimulus than 20-Hz oscillatory stimulation (Figures 5A and 5B). Importantly, shuffling the phases of the optical stimulus abolished phase locking to the optical stimulus, demonstrating that the effects were not due to chance, even in the baseline condition (Figure 5C). Moreover, no phase locking to the optical stimulus was observed in non-opsin controls (Figure S4B). Interestingly, phase locking of mPFC units to the 8-Hz optical stimulus was significantly stronger when mice were in the open arms compared to the closed arms; this open arm entrainment was not seen in mice receiving 20-Hz stimulation (Figure 5D). Together, these data demonstrate that, although oscillatory stimulation of vHPC inputs at either 8 or 20 Hz is capable of entraining mPFC neuronal activity *in vivo*, entrainment to theta-frequency stimulation is preferentially enhanced in anxiogenic environments.

Prior work suggests that vHPC inputs send task-relevant information to the mPFC that is used to guide avoidance behavior (Adhikari et al., 2011; Ciocchi et al., 2015; Padilla-Coreano et al., 2016). Exogenous stimulation might be expected to interfere with this signal. Yet here, exogenous oscillatory stimulation increases avoidance behavior (Figure 1). This finding suggests that the oscillatory stimulation facilitates information flow through the vHPC-mPFC pathway, perhaps by facilitating the ability of properly timed vHPC input to drive mPFC neurons. To investigate whether our oscillatory 8-Hz stimulation indeed enhanced the ability of mPFC neurons to follow properly timed vHPC activity, we recorded vHPC LFPs in a subset of mice while optogenetically stimulating vHPC-mPFC terminals (Figure S5A). We quantified phase locking of mPFC single units to vHPC theta (4–12 Hz) in behaving mice during the EPM. Because 8-Hz stimulation decreased the time spent in the open arms, limiting the duration of our neural recordings in the open arms, we matched the number of spikes per unit in both open and closed arms to compare phase locking strength across conditions (see STAR Methods for details). Similar to phase locking to the optical stimulus, phase locking to vHPC theta was increased by 8-Hz (and not 20-Hz) oscillatory stimulation only in the open arms of the EPM (Figure 6A). These data suggest that our manipulation indeed synchronizes mPFC spiking to ongoing vHPC theta in anxiogenic environments.

But how is it that 8-Hz oscillatory stimulation entrains mPFC spiking to ongoing vHPC activity? One explanation is that the optical stimulus entrains vHPC activity itself, either through activation of indirect pathways that feed back to the vHPC or through direct retrograde activation of vHPC neurons. Entrainment was quantified by computing coherence between the ongoing vHPC LFP and the oscillatory stimulus. Indeed, we found that the oscillatory stimulus entrained the vHPC, as moderate levels of coherence were seen between the vHPC LFP and the optical stimulus during EPM exploration, only in ChR2-expressing animals (Figures 6B and S5B). Entrainment of the vHPC local field potential to the 8-Hz oscillatory stimulus was present throughout the maze, though modestly stronger in the closed arms compared to the open arms (Figure 6C). This finding is consistent with previous reports that vHPC theta power is higher in the closed arms (Adhikari et al., 2010) and supports the idea that, with vHPC, theta reflects behavioral inhibition. Coherence

shown. Firing is normalized by subtracting the mean evoked firing for 10–40 ms post-electrical stimulation in the absence of light (n = 50 single units; Wilcoxon signed-rank $^{**}p < 0.01$, $^{***}p < 0.001$).

(F) Normalized evoked firing rates for 20-Hz versus 8-Hz oscillatory stimulation at 90° < phase < 180° (n = 50 single units; Wilcoxon signed-rank $^{**}p = 0.01$). Error bars indicate SEM.

See also Figure S3.

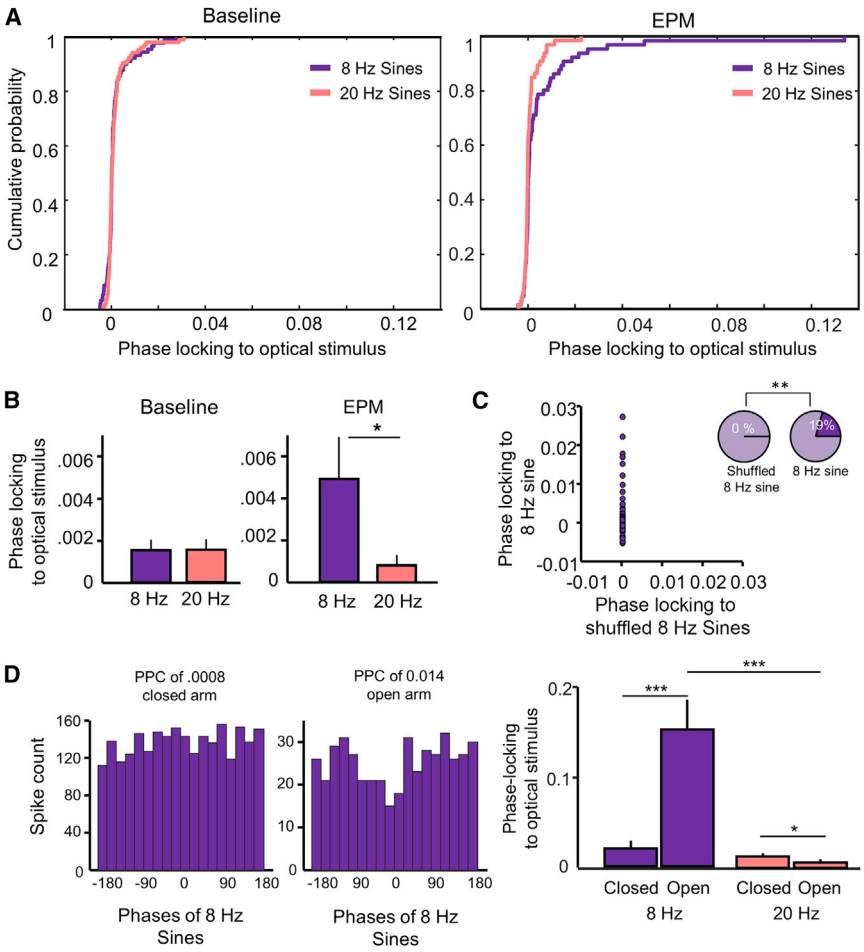

Figure 5. mPFC Entrainment to the 8-Hz Oscillatory Stimulus Is Enhanced in an Anxiogenic Environment.

(A) Cumulative distribution of the strength of phase locking of mPFC single units to the oscillatory optical stimulus at 8 and 20 Hz in a baseline condition (left) and during the EPM test (right).

(B) (Left) Average mPFC phase locking to the oscillatory optical stimulus in a baseline condition for 8 and 20 Hz (8 Hz n = 90 single units; 20 Hz n = 112 single units; Wilcoxon rank-sum p = 0.93). (Right) Average mPFC phase locking to the oscillatory optical stimulus in the EPM for 8-Hz sines and 20-Hz sines (left panel, 8 Hz n = 66 single units; 20 Hz n = 57 single units; Wilcoxon rank-sum *p = 0.03).

(C) Scatterplot showing phase locking of mPFC single units to 8-Hz oscillatory optical stimulus at baseline versus phase locking to 8-Hz stimulus after shuffling the sine phases. Pie chart shows % phase-locked units to 8-Hz oscillatory stimulus vs shuffled stimulus (8 Hz versus shuffled two-sample chi-square **p < 0.01).

(D) (Left) Distribution of phases for spikes of example unit to 8-Hz oscillatory stimulus in the open versus closed arms. (Right) Phase locking strength to the oscillatory stimulus as measured with pairwise phase consistency in the open or closed arms for 8-Hz (n = 39) and 20-Hz stimulation (n = 42) is shown (only units that met spike number criteria were included in this analysis; see details in STAR Methods; 8 Hz open versus closed ***p < 0.0001; 20 Hz open versus closed *p = 0.03; open arms 8 versus 20 Hz ***p < 0.0001; closed arms 8 versus 20 Hz p = 0.40). Error bars indicate SEM. See also Figure S4.

between the 8-Hz optical stimulus and the vHPC LFP increased over the first few seconds of light presentation (Figure 6D), suggesting some recruitment of indirect feedback into vHPC via the extended circuit. Interestingly, during the first few seconds following light onset of 8-Hz oscillatory stimulation, the probability that mice were in an open arm decreased with a time course that matched that of the increased coherence (Figure 6E). These findings suggest that entrainment of vHPC activity to the 8-Hz oscillatory stimulation contributes to the observed increase in avoidance behavior (Figure 1).

To determine whether 8-Hz oscillatory terminal stimulation entrained vHPC activity via direct backpropagation, we compared vHPC single-unit activity after pulsatile and oscillatory stimulation of vHPC terminals. We posited that, because pulsatile optical stimulation results in backpropagation (Ciocchi et al., 2015), we could use pulse-evoked vHPC antidromic activation as a positive control to determine whether oscillatory optical stimulation also generates backpropagation. After expressing ChR2 in the vHPC, recordings were made during anesthesia with a silicon probe in the pyramidal layer of the vHPC for high-density, single-unit recording while light was delivered via a fiber optic in the mPFC. To compare responses evoked by the two different stimuli, we first determined which vHPC units were activated by terminal stimulation in the 8-Hz pulse condition. Our criteria for considering a cell to be activated via backpropagation were based on a classification protocol for vHPC (Ciocchi et al., 2015); vHPC cells had to spike with low jitter to the pulse (high precision; all responses occurring within $\leq$0.3 ms of each other) and with high fidelity (greater than or equal to 90%; Figures S6A and S6B). In the vast majority of the single units, we saw no evidence of activation by pulsatile light (256/329 units; Figure S6C). In ~2% of the units (8/329), we saw activation to the light pulses that was consistent with direct effects of backpropagation (Figure S6C). No units had significant antidromic activity during the oscillatory stimulation (Figure S6C). A larger subset of units (20% for pulses: 73/329; 1.5% for sines: 5/329) showed increased jitter in their response with slower activation, consistent with synaptic activation via feedforward activation. On average, pulsatile stimulation caused more spiking than oscillatory stimulation for both antidromic and synaptic activation (Figure S6D). Consistent with these findings, in the awake brain, pulsatile stimulation induced strong, robust field potential responses in the vHPC, and oscillatory stimulation induced significantly smaller responses at peak light output, suggesting it evoked weaker activation of vHPC than pulsatile stimulation (Figure S6E). Taken together, these data demonstrate that 8-Hz oscillatory stimulation increases vHPC-mPFC synchrony, not via direct backpropagation but by engaging vHPC indirectly.

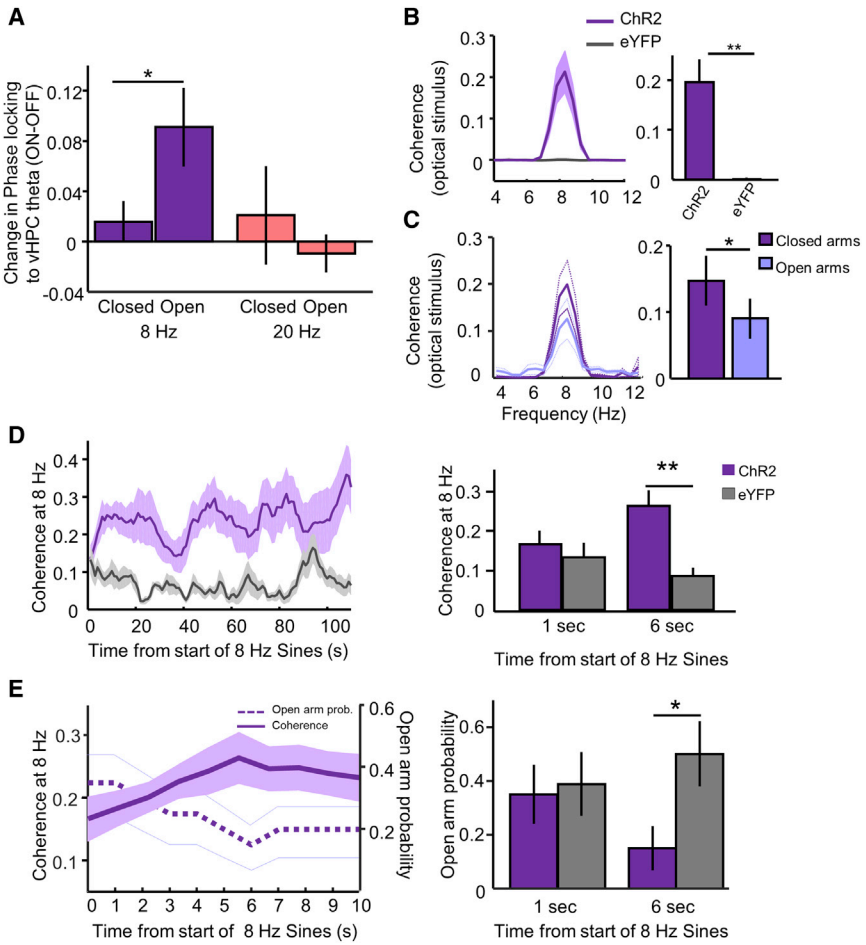

Figure 6. vHPC-mPFC Theta Synchrony Is Enhanced and Entrained by the 8-Hz Oscillatory Stimulation during Avoidance Behavior

(A) Change in phase-locking strength (light ON – light OFF) for mPFC units to vHPC theta (4–12 Hz) during exploration of open and closed arms of the EPM (8 Hz n = 36; 20 Hz n = 27; Wilcoxon signed-rank test for closed versus open for 8 Hz p = 0.017).

(B) (Left) Mean coherence between the vHPC LFP and the 8-Hz oscillatory stimulus (ChR2 n = 8 animals; non-opsin n = 6 animals). (Right) Average coherence at 7–9 Hz between the vHPC LFP and 8-Hz oscillatory stimulation is shown (ChR2 n = 8, eYFP n = 6; Wilcoxon rank-sum, **p = 0.01).

(C) (Left) Coherence between vHPC LFP and the oscillatory stimulus in closed versus open arms for the ChR2 group. (Right) Average coherence at 7–9 Hz for closed versus open arms (n = 8; Wilcoxon signed-rank closed versus open arms *p = 0.015).

(D) (Left) Coherence between the vHPC LFP and the 8-Hz oscillatory optical stimulus over time. (Right) Average coherence at 1 and 6 s (Wilcoxon rank-sum ChR2 versus eYFP at 6 s, **p = 0.0016).

(E) (Left) Coherence between the vHPC LFP and the 8-Hz oscillatory optical stimulus and open arm probability for mice expressing ChR2 during the first 10 s of light stimulation (for coherence ChR2 n = 8, eYFP n = 6; for behavior ChR2 n = 10, eYFP = 9, two light ON epochs per mouse used). (Right) Average open arm probability at 1 and 6 s (two light ON epochs used per mouse; ChR2 n = 10, eYFP = 9; Wilcoxon rank-sum ChR2 versus eYFP at 6 s, *p = 0.023). Error bars indicate SEM. See also Figures S5 and S6.

DISCUSSION

We have demonstrated the specific causal relevance of theta-frequency activity in the vHPC-mPFC circuit during avoidance behaviors, as optogenetic oscillatory stimulation of the vHPC-mPFC projection at 8 Hz, but not 20 Hz, maximally enhanced vHPC-mPFC synchrony and transmission, entrained mPFC neurons, and increased avoidance behavior. These findings, combined with prior results (Padilla-Coreano et al., 2016; Parfitt et al., 2017), collectively demonstrate bidirectional effects of manipulating the vHPC-mPFC circuit and point to a privileged role for theta-frequency activity in sustaining information transfer within this circuit. Intriguingly, because many of our effects were specific to oscillatory, but not pulsatile, stimulation, our results suggest that the light pattern during an optogenetic manipulation is as important as the frequency of stimulation. Our results support a sequence of mechanisms by which the oscillatory optical pattern delivered at 8 Hz may enhance this information transfer. Our data further suggest that 8-Hz oscillatory stimulation first facilitates mPFC postsynaptic responses to vHPC input and next enhances vHPC-mPFC synchrony via indirect projections as opposed to backpropagation.

Oscillatory facilitation of mPFC responses to vHPC stimulation was demonstrated both by increased spontaneous-like EPSCs *ex vivo* and facilitated neurotransmission of vHPC-mPFC pathway during vHPC electrical stimulation *in vivo*. Interestingly, 8-Hz pulsatile stimulation had the strongest light-evoked EPSCs *ex vivo* but did not evoke changes in avoidance behavior and did not facilitate vHPC-evoked responses in mPFC. We hypothesize that, although pulses, given their fast rise time, are more efficient at driving the terminals to fire simultaneously, they drive the postsynaptic neurons in a way that fails to convey relevant information about the animal's environment. By contrast, delivering photons with the slower rise time of the oscillatory stimulation seems to produce less synchronous activation of the terminals, which may not drive action potentials significantly in the vHPC terminals. This is shown by the nature of the mPFC responses in our *ex vivo* experiments. We hypothesize instead that the exogenous oscillatory stimulation biases release, increasing the likelihood that vHPC activity successfully drives mPFC responses and facilitating information flow through these synapses. The finding that oscillatory stimulation increased mPFC-evoked responses to vHPC electrical stimulation is consistent with this hypothesis. Together, our findings suggest that oscillatory stimulation facilitates the transmission of appropriately timed information arriving from the vHPC during behavior.

This increased vHPC-mPFC transmission in turn facilitated theta synchrony between the vHPC and mPFC during avoidance

behavior. Our results showed that 8-Hz oscillatory stimulation entrained mPFC spiking and vHPC theta activity to the light stimulus and increased synchrony between vHPC theta and mPFC spiking. Prior work has described correlations between increased mPFC and vHPC theta synchrony and increased avoidance behavior (Adhikari et al., 2010, 2011). By introducing an optogenetic oscillatory stimulation paradigm that is capable of exogenously increasing vHPC-mPFC theta synchrony, we found increases in avoidance behavior, lending further support to a causal relationship between vHPC-mPFC theta synchrony and avoidance behavior. How 8-Hz oscillatory stimulation entrains the vHPC-mPFC circuit remains unclear, but our data suggest it is not via direct backpropagation. We found that although 2% of vHPC cells had antidromic activation to pulsatile stimulation, none had significant antidromic activation to oscillatory stimulation of mPFC terminals. One likely possibility is that, because the mPFC does not directly project to vHPC, a feedforward pathway entrains vHPC neurons via activation of the mPFC and its (indirect) projections to the hippocampus, perhaps through the thalamus, amygdala, or entorhinal cortex.

Intriguingly, the effects of 8-Hz oscillatory stimulation on vHPC-mPFC synchrony depended on the behavioral state. Synchrony between mPFC neuron spiking and the 8-Hz optical stimulus was enhanced during exposure to the EPM and was strongest in the open arms of the EPM, suggesting an interaction between the optogenetic stimulation and some intrinsic physiological response engaged by the anxiogenic environment. Moreover, 8-Hz oscillatory stimulation preferentially enhanced synchrony between mPFC unit spiking and vHPC theta activity during exploration of the open arms, consistent with the notion that this interaction occurs at the level of mPFC responsiveness to vHPC input. One candidate mechanism for this interaction could be changes in serotonergic signaling in the mPFC, as recent studies have demonstrated that serotonin can gate vHPC-mPFC neurotransmission and theta activity during avoidance behaviors via presynaptic 5-HT_{1B} receptors (Kjaerby et al., 2016). Recent work demonstrated that local vasoactive intestinal polypeptide (VIP) interneurons disinhibit mPFC responses to vHPC input, and VIP interneuron activity is necessary for mPFC neural representations of the open arms in the EPM (Lee et al., 2019). Moreover, inhibition of VIP interneuron activity maximally affected avoidance behavior when vHPC-mPFC theta synchrony was highest, suggesting that vHPC theta activity recruits mPFC VIP neurons to induce avoidance (Lee et al., 2019). Therefore, potential recruitment of mPFC VIP interneurons during our 8-Hz oscillatory stimulation may underlie the strong increases in vHPC-mPFC theta synchrony observed in our study, particularly in the open arms. Future work might explore this hypothesis.

One remaining question is whether the vHPC-mPFC circuit preferentially engages with 8-Hz stimulation because of biophysical limitations or whether it might be engaged at other frequencies to drive distinct behaviors. Our findings suggest that 8 Hz plays a privileged role in enhancing vHPC-mPFC neurotransmission and avoidance behavior. However, other *in vivo* physiology studies have found that the mPFC and vHPC synchronize in the gamma frequency during encoding of a working memory task (Spellman et al., 2015), providing evidence that the same circuit might produce distinct behaviors when engaged at different frequencies.

The privileged capacity of 8-Hz activity in the vHPC-mPFC pathway to enhance neurotransmission and avoidance behavior was further supported by our findings using 4-Hz and 2-Hz stimulation. 4-Hz stimulation produced inconsistent effects on measures of avoidance behavior and decreased locomotion, and 2-Hz stimulation failed to increase avoidance. Interestingly, oscillatory optogenetic stimulation of mPFC interneurons at 4 Hz has been shown to increase freezing and fear behavior, and no such behavioral effect was observed with stimulation at 8 Hz (Karalis et al., 2016). Our findings, together with the Karalis study, suggest that frequency-specific manipulations of distinct circuit components in the mPFC recruit distinct neural oscillations with distinct behavioral outcomes.

In conclusion, in addition to showing that theta-frequency activity plays a preferential, causal role in vHPC-mPFC communication during avoidance behavior, our findings more broadly highlight the importance of studying frequency-specific oscillations as an important dimension in our quest to understand how the brain produces behavior.

STAR★METHODS

Detailed methods are provided in the online version of this paper and include the following:

- KEY RESOURCES TABLE
- LEAD CONTACT AND MATERIALS AVAILABILITY
- EXPERIMENTAL MODEL AND SUBJECT DETAILS
  - Animal Subjects
  - Viral Constructs
- METHOD DETAILS
  - Surgical Procedures
  - Behavioral procedures
  - In vivo electrophysiology
  - Anesthetized in vivo electrophysiology
  - Ex vivo electrophysiology
- QUANTIFICATION AND STATISTICAL ANALYSIS
  - Behavioral analysis
  - In vivo electrophysiology
  - Ex vivo electrophysiology
- DATA AND CODE AVAILABILITY

SUPPLEMENTAL INFORMATION

Supplemental Information can be found online at https://doi.org/10.1016/j.neuron.2019.08.006.

ACKNOWLEDGMENTS

We thank William Hardin, Zachary Bretton, and Eric Myhre for technical support. We thank Dr. Alexander Harris for intellectual input. We thank all members of the Gordon lab for useful feedback. We thank the reviewers for useful feedback. Funding was provided from a National Science Foundation Graduate Student Fellowship (to N.P.-C. during her time at Columbia) and grants from the International Mental Health Research Organization (J.A.G.), the Hope for Depression Research Foundation (J.A.G.), and the NIMH: R01-MH096274 and R01-MH081968 to J.A.G. during his time at Columbia; K01 MH107760 and a Brain and Behavior Research Foundation Young Investigator

Award to S.C.; R01-MH102441 to K.M.T.; and R21-MH117454 to C.K. A.L.G.-G. was supported by Spain Science Department and Sackler Institute fellowships. J.A.G., R.M.M., E.A., M.V.M., S.H., and D.A.K. are supported by the NINDS intramural research program (ZIA NS003168). N.P.-C. is supported by a postdoctoral fellowship of the Simons Center for the Social Brain and a Ford Foundation postdoctoral fellowship.

AUTHOR CONTRIBUTIONS

N.P.-C. and J.A.G. designed the overall study. Experimental design was done by N.P.-C., J.A.G., S.C., C.K., D.A.K., and K.M.T. Data collection and analysis were supervised by N.P.-C., S.C., and D.A.K. Surgeries were done by N.P.-C., S.C., R.W., D.R.B., A.L.G.-G., M.P.M., R.M.M., E.A., J.P., S.H., E.T., and M.V.M. Hardware and software integration for oscillatory light control was done by R.W. and M.V.M. Behavioral data collection was done by N.P.-C., A.L.G.-G., S.C., M.P.M., D.R.B., R.W., E.T., R.M.M., E.A., and S.H. and analyzed by N.P.-C., S.C., E.T., R.M.M., and E.A. Histology was done by D.R.B., R.W., R.M.M., E.A., S.C., N.P.-C., and D.A.K. *Ex vivo* electrophysiology experiments were done and analyzed by S.C. *In vivo* electrophysiology data were collected and analyzed by N.P.-C. and J.P. Figures were made by N.P.-C., S.C., R.M.M., E.A., and J.P. Data were interpreted by N.P.-C., C.K., J.A.G., S.C., D.A.K., J.P., R.M.M., and E.A. The manuscript was written by N.P.-C., S.C., and D.A.K. and edited by J.A.G., C.K., and K.M.T.

DECLARATION OF INTERESTS

The authors declare no competing interests.

Received: July 25, 2018
Revised: June 8, 2019
Accepted: August 3, 2019
Published: September 11, 2019

REFERENCES

Adhikari, A., Topiwala, M.A., and Gordon, J.A. (2010). Synchronized activity between the ventral hippocampus and the medial prefrontal cortex during anxiety. Neuron *65*, 257–269.

Adhikari, A., Topiwala, M.A., and Gordon, J.A. (2011). Single units in the medial prefrontal cortex with anxiety-related firing patterns are preferentially influenced by ventral hippocampal activity. Neuron *71*, 898–910.

Buzsáki, G., and Watson, B.O. (2012). Brain rhythms and neural syntax: implications for efficient coding of cognitive content and neuropsychiatric disease. Dialogues Clin. Neurosci. *14*, 345–367.

Buzsáki, G., Anastassiou, C.A., and Koch, C. (2012). The origin of extracellular fields and currents–EEG, ECoG, LFP and spikes. Nat. Rev. Neurosci. *13*, 407–420.

Ciocchi, S., Passecker, J., Malagon-Vina, H., Mikus, N., and Klausberger, T. (2015). Brain computation. Selective information routing by ventral hippocampal CA1 projection neurons. Science *348*, 560–563.

Harris, A.Z., and Gordon, J.A. (2015). Long-range neural synchrony in behavior. Annu. Rev. Neurosci. *38*, 171–194.

Karalis, N., Dejean, C., Chaudun, F., Khoder, S., Rozeske, R.R., Wurtz, H., Bagur, S., Benchenane, K., Sirota, A., Courtin, J., and Herry, C. (2016). 4-Hz oscillations synchronize prefrontal-amygdala circuits during fear behavior. Nat. Neurosci. *19*, 605–612.

Kjaerby, C., Athilingam, J., Robinson, S.E., Iafrati, J., and Sohal, V.S. (2016). Serotonin 1B receptors regulate prefrontal function by gating callosal and hippocampal inputs. Cell Rep. *17*, 2882–2890.

Lee, A.T., Cunniff, M.M., See, J.Z., Wilke, S.A., Luongo, F.J., Ellwood, I.T., Ponnavolu, S., and Sohal, V.S. (2019). VIP interneurons contribute to avoidance behavior by regulating information flow across hippocampal-prefrontal networks. Neuron *102*, 1223–1234.e4.

Likhtik, E., Stujenske, J.M., Topiwala, M.A., Harris, A.Z., and Gordon, J.A. (2014). Prefrontal entrainment of amygdala activity signals safety in learned fear and innate anxiety. Nat. Neurosci. *17*, 106–113.

Padilla-Coreano, N., Bolkan, S.S., Pierce, G.M., Blackman, D.R., Hardin, W.D., Garcia-Garcia, A.L., Spellman, T.J., and Gordon, J.A. (2016). Direct ventral hippocampal-prefrontal input is required for anxiety-related neural activity and behavior. Neuron *89*, 857–866.

Parfitt, G.M., Nguyen, R., Bang, J.Y., Aqrabawi, A.J., Tran, M.M., Seo, D.K., Richards, B.A., and Kim, J.C. (2017). Bidirectional control of anxiety-related behaviors in mice: role of inputs arising from the ventral hippocampus to the lateral septum and medial prefrontal cortex. Neuropsychopharmacology *42*, 1715–1728.

Pérez-Escudero, A., Vicente-Page, J., Hinz, R.C., Arganda, S., and de Polavieja, G.G. (2014). idTracker: tracking individuals in a group by automatic identification of unmarked animals. Nat. Methods *11*, 743–748.

Spellman, T., Rigotti, M., Ahmari, S.E., Fusi, S., Gogos, J.A., and Gordon, J.A. (2015). Hippocampal-prefrontal input supports spatial encoding in working memory. Nature *522*, 309–314.

Tierney, P.L., Thierry, A.M., Glowinski, J., Deniau, J.M., and Gioanni, Y. (2008). Dopamine modulates temporal dynamics of feedforward inhibition in rat prefrontal cortex in vivo. Cereb. Cortex *18*, 2251–2262.

Uhlhaas, P.J., and Singer, W. (2012). Neuronal dynamics and neuropsychiatric disorders: toward a translational paradigm for dysfunctional large-scale networks. Neuron *75*, 963–980.

Vinck, M., van Wingerden, M., Womelsdorf, T., Fries, P., and Pennartz, C.M.A. (2010). The pairwise phase consistency: a bias-free measure of rhythmic neuronal synchronization. Neuroimage *51*, 112–122.

STAR★METHODS

KEY RESOURCES TABLE

REAGENT or RESOURCE	SOURCE	IDENTIFIER
Bacterial and Virus Strains		
AAV5-CaMKIIa-hChR2(H134R)-mCherry	UNC Vector Core	https://www.med.unc.edu/genetherapy/vectorcore/in-stock-aav-vectors
AAV5-CaMKIIa-mCherry	UNC Vector Core	https://www.med.unc.edu/genetherapy/vectorcore/in-stock-aav-vectors
AAV5-CaMKIIa-eYFP	UNC Vector Core	https://www.med.unc.edu/genetherapy/vectorcore/in-stock-aav-vectors
AAV5-CaMKIIa-hChR2(H134R)-EYFP	Addgene	https://www.addgene.org/26969/
Isolectin GS-IB4, Alexa Fluor™ 647	ThermoFisher Scientific	https://www.thermofisher.com/order/catalog/product/I32450
NeuroTrace™ 435/455 Blue Fluorescent Nissl Stain	ThermoFisher Scientific	https://www.thermofisher.com/order/catalog/product/N21479
Chicken anti-GFP antibody	Abcam	https://www.abcam.com/gfp-antibody-ab13970.html; RRID: AB_2543096
Alexa Fluor 488 goat anti-chicken secondary antibody	ThermoFisher Scientific	https://www.thermofisher.com/antibody/product/Goat-anti-Chicken-IgY-H-L-Secondary-Antibody-Polyclonal/A-11039; RRID: AB_2534096
Experimental Models: Organisms/Strains		
129SvevTac mice	Taconic Farms	https://www.taconic.com/mouse-model/129s6
Software and Algorithms		
MATLAB	Mathworks	https://www.mathworks.com/products/matlab.html
Python	Anaconda	https://www.anaconda.com/distribution/
IdTracker	De Polavieja Lab, Cajal Institute	http://www.idtracker.es/home
CowLog	CowLog	http://cowlog.org/
SpikeSort 3D	Neuralynx	https://neuralynx.com/software/spikesort-3d
Clampfit	Molecular Devices	https://www.moleculardevices.com/products/axon-patch-clamp-system/acquisition-and-analysis-software/pclamp-software-suite
MiniAnalysis	Synaptosoft	http://www.synaptosoft.com/MiniAnalysis/
Prism	GraphPad	https://www.graphpad.com/scientific-software/prism/

LEAD CONTACT AND MATERIALS AVAILABILITY

Further information and requests for resources and reagents should be directed to and will be fulfilled by the Lead Contact Joshua Gordon (joshua.gordon@nih.gov).

EXPERIMENTAL MODEL AND SUBJECT DETAILS

Animal Subjects

All procedures were conducted in accordance with the U.S. NIH Guide for the Care and Use of Laboratory Animals and the New York State Psychiatric Institute Institutional Animal Care and Use Committees at Columbia University. 100 adult male 129SvevTac mice were purchased from Taconic Farms and surgerized between 8-10 weeks of age.

Viral Constructs

For optogenetic manipulations, adeno-associated viruses (AAV; ~4-8x10^{12} μg/ml, unless indicated differently) were obtained from the University of North Caroline Vector Core Facility and Addgene. Viruses were kept at -80° C until use. We saw no evidence of anterograde or retrograde expression of our AAV constructs (i.e. no observed somatic expression outside of the vHPC).

METHOD DETAILS

Surgical Procedures

For the behavior experiments (8 Hz and 20 Hz), 83 male adult 129SvevTac mice between 8-10 weeks of age were bilaterally infected with either AAV5-CaMKIIa-hChR2(H134R)-mCherry, or AAV5-CaMKIIa–eYFP or CaMKIIa-mCherry into the vHPC under ketamine/xylazine or isoflurane anesthesia. 200 nl of virus was pressure-injected through a glass micropipette at each injection site at a rate of 200nl/min. In each hemisphere, five injections were done at -3.10 and at -3.30 AP levels for a total of 10 injections per hemisphere. At each AP level, the five injection sites were ±2.90, -4.0; ±3.30, -3.60; ±3.30 -1.7; ±3.70, -3.2; ±3.70, -2.50 (ML and DV, respectively). For the 4-Hz and 2-Hz behavioral experiments, 16 male adult 129SvevTac mice between 8-10 weeks of age were bilaterally injected with AAV5-CaMKIIa-hChR2(H134R)-eYFP into the vHPC under isoflurane anesthesia. 300nl of 10^{13} μg/ml virus was pressure-injected through a glass micropipette at each injection site at a rate of 100nl/min. In each hemisphere, four injections were made at two AP sites and two depths for each site (-3.00 AP, ±2.75 ML, -3.85 and -3.25 DV) and (-3.30 AP, ±3.25 ML, -3.10 and -2.50 DV). Coordinates are in mm relative to Bregma (AP, ML) or brain surface at the most medial coordinate (DV). 6 weeks after viral infection, a subset of mice was surgically implanted with electrodes and optical fibers, also under ketamine/xylazine or isoflurane anesthesia. Stereo-optrodes were implanted in the mPFC (1.60 AP, ±0.4 ML and -1.25 DV), mice that had optical fibers only had fibers implanted during injection surgery into mPFC bilaterally using the same coordinates as stereo-optrodes. Each stereo-optrode was comprised of a 230-μm optical fiber glued to a bundle of 14 tungsten wire (13-μm diameter) stereotrodes placed 400–500 μm below the end of the optical fiber (Padilla-Coreano et al., 2016). 75-μm diameter tungsten wire LFP electrodes were implanted in the CA1 region of the vHPC (-3.30 AP, ±3.30 ML, -3.60 DV). A reference screw was implanted in the skull at a site roughly above frontal cortex/olfactory bulb area, and a ground screw was implanted at a site roughly above the cerebellum (behind lambda). Mice were allowed to recover from electrode implantation for at least 10 days before behavioral habituation began.

Behavioral procedures

EPM behavioral protocol: Seven to eight weeks after viral infection mice were food restricted to 80% of pre-operative weight and habituated to the opto/electrical tether in a small dark wooden box (20x3x30 cm; referred to as familiar box in text) as they foraged for food pellets. After 3 days of habituation in the familiar box, mice were placed in the center of the EPM facing an open arm under ~200 lux of illumination in the room. Nine out of 79 mice in the 8- and 20-Hz cohorts were excluded from behavioral analysis for not moving in the EPM from a single compartment throughout the duration of the experiment. The same group of mice was used to assess the impact of 4-Hz and 2-Hz oscillatory stimulation. Mice were first tested at 4-Hz stimulation and three weeks later were tested at 2-Hz stimulation. All habituation and food restriction procedures were repeated leading up to the second test. Seven (4-Hz) to ten (2-Hz) weeks after viral injection mice were food restricted to 80% of pre-operative weight and habituated to the optical tether in their home cage as they foraged for food pellets. After 3 days of habituation in the home cage, mice were placed in the EPM under ~100 lux of illumination. Mice were introduced to the maze in the center facing the same open arm. For this experiment, some mice were excluded for the following reasons: being introduced to the EPM facing a closed arm (4 Hz: n=1), seizures (2 Hz: n=3, 4 Hz: n=1), bleeding from implant (2 Hz: n=1), and errant fiber placement (2 Hz: n=1, 4 Hz: n=1). Video recordings of EPM trials were captured for subsequent behavioral scoring using an overhead camera (2-and 4-Hz experiments: BFLY-U3-13S2C, Blackfly; Spinnaker SDK, FLIR; 8 and 20 Hz experiments: SV-C3200, jAi).

Light stimulation during behavior: The LED (465 nm; PlexBright LD-1 Single Channel LED Driver; Plexon) light output was controlled with an Arduino uno device and custom code and sent to the LED via the analog channel to deliver pulses or sinusoids of 465 nm at 8-10 mW as measured at the end of the patchcord (for Figures 1 and S1 experiments). Importantly, the peak power of the 8 Hz pulses and 8 Hz sinusoids matched. For the 4- and 2-Hz behavioral experiments, an oscillatory laser output (473 nm; Cobolt Modulated Laser Diode; 8-11 mW at peak from the tip of a representative fiber implant) was achieved using a Blackrock Microsystems computer interface and custom Python code. For all experiments light was delivered in 2-min epochs for 8 minutes.

In vivo electrophysiology

Data were acquired using a Digital Lynx system (Neuralynx). To record vHPC local field potentials (LFP) the tungsten electrode was referenced to a screw located in the skull over the frontal cortex/olfactory bulb, band-pass filtered (1–1000 Hz), and acquired at 2 kHz as previously described (Padilla-Coreano et al., 2016). The Arduino signal that controlled the LED light output was recorded in order to calculate the phases and timing of the optical stimulation signal delivered into the mPFC. Single unit mPFC recordings were band-pass filtered at 600–6000 Hz and acquired at 32 kHz; spikes were detected by thresholding and sorted offline as previously described (Padilla-Coreano et al., 2016). Only single units with at least 100 spikes per light condition (>0.4 Hz) were included in phase-locking analyses of whole EPM test sessions. For analyses that looked at compartment differences in phase locking, only single units with at least 70 spikes per compartment/light condition were included. Moreover, the number of spikes used for the open and closed arms

was matched per single unit. To get a good estimation of the phase locking with a subsample of spikes, we repeated the calculation 500 times with a different subset of spikes and averaged the phase locking value. For vHPC field analyses, mice were recorded in a familiar box in the dark while pulses or oscillatory light were delivered in the mPFC. Raw vHPC LFP was aligned around each cycle of light and averaged across light cycles to quantify the evoked vHPC response. There was no difference between the evoked response to pulses and oscillatory light in non-opsin mice (rank-sum p=0.92). Controls plotted in evoked potential Figure S6E correspond to oscillatory light in non-opsin mice.

Anesthetized in vivo electrophysiology

Five mice were injected with AAV5-CaMKIIa-hChR2(H134R)-mCherry bilaterally into the vHPC as indicated in the surgical procedures. After 7-8 weeks for viral expression mice were anesthetized with isoflurane and an electrical stimulating tungsten electrode (World Precision Instruments) was stereotaxically placed into the vHPC while an optrode (stereotrodes glued to a fiber) was placed into the mPFC (AP +1.6-1.8 ML 0.3 DV -1.5-2). mPFC single unit recordings were conducted with a Neuralynx system as described above. Once single units were found in mPFC, the vHPC electrode was advanced within the vHPC until an evoked response was detected on the single units in the mPFC. While searching for units with evoked responses, electrical stimulation was ramped up to a max of 500 μA for 0.1 ms, and later lowered between 200-400 μA to achieve a non-maximal response. For the remainder of the experiment the stimulation strength was constant. Once mPFC units with vHPC responses were found, the experiment began. Each experimental session included trials of vHPC electrical stimulation alone (with a pseudorandom ITI between 1.5 to 2.5 s) and the same electrical stimulation combined with vHPC terminal photostimulation in mPFC with the following optical patterns: 8 Hz pulses, 8 Hz sinusoids and 20 Hz sinusoids (see Figures 3 and S3). The order of the optical patterns presented was counterbalanced across experiments (e.g. recording sessions). Population averages in Figures 3 and S3 include all recorded mPFC single units regardless of how strongly or weakly they responded to the vHPC electrical stimulation. For cross-light patterns and cross-phase analyses, only single units that were recorded under all optical patterns were included. To do phase analysis on pulses we assigned pseudo-phases to the 125 ms surrounding the pulse. The peak of the pulse was assigned as phase 0 to be equivalent with the peak of the sine wave (see Figure S3E).

Acute vHPC neuronal recordings (Blackrock Microsystems) were performed with a 32-channel silicon probe (Cambridge Neurotech) in an isoflurane-anesthetized mouse expressing ChR2 in vHPC inputs to the mPFC and implanted with bilateral optical fibers in the mPFC. The probe was slowly advanced into the vHPC and screening for the presence of neuronal activation commenced following mPFC optical stimulation. In total, 329 units were identified. Pulse stimulations lasted for 12.5 s and consisted of 100, 5-ms pulses delivered at 8 Hz. Sine wave stimulations were conducted using a matching frequency, duration and peak light intensity. Intermixed were light-off periods of the same 12.5 s duration to record baseline activity. Neuronal spiking activity was clustered via Kilosort and neuronal spike timings analyzed with custom-written Matlab code (Matlab 2018a). To classify vHPC responses to 8 Hz pulses as antidromic (thus activated via direct backpropagation from stimulated terminals) we followed the classification process of a previous study (Ciocchi et al., 2015). vHPC neurons that responded with low jitter $\leq$0.3 ms (all responses occurring within 0.3 ms of each other from light onset) and a response fidelity of $\geq$ 90% within a given 100-pulse stimulus episode were classified as antidromically activated (n=8 units). Collisions could not be tested due to extremely low firing rates during anesthesia. Some vHPC neurons had a longer-latency activation by the optogenetic stimulation that was too slow to be antidromic. These diverse longer-latency, putative synaptic responses were classified based on having response jitter between 0.3-5 ms and a minimum firing rate of 1 Hz during the response interval (0-125 ms; 0 is pulse onset). If a cell did not meet criteria for either antidromic or synaptic responses, it was considered non-responsive (n=256). For each response classification group, we report average firing rates for the population during the whole 0-125 ms during pulse trials vs oscillatory trials.

Ex vivo electrophysiology

Whole-cell voltage clamp recordings were made from layer 3/5 pyramidal cells in the prelimbic (PrL) region of the mPFC. Recordings were obtained with a Multiclamp 700B amplifier (Molecular Devices, Sunnyvale, CA, USA) and digitized using a Digidata 1440A acquisition system (Molecular Devices) with Clampex 10 (Molecular Devices). Following decapitation, 300-μM slices containing the mPFC were incubated in artificial cerebral spinal fluid containing (in mM): 126 NaCl, 2.5 KCl, 2.0 $MgCl_2$, 1.25 $NaH2PO_4$, 2.0 $CaCl_2$, 26.2 $NaHCO_3$ and 10.0 D-glucose, bubbled with oxygen, at 32° C for 30 min before being returned to room temperature for at least 30 min prior to use. During recording, slices were perfused in artificial cerebral spinal fluid (with drugs added as detailed below) at a rate of 5 ml min^{-1}. Electrodes were pulled from 1.5 mM borosilicate-glass pipettes on a P-97 puller (Sutter Instruments, Novato, CA, USA). Electrode resistance was typically 3–5MΩ when filled with internal solution consisting of (in mM): 130 K-gluconate, 5 NaCl, 10 HEPES, 0.5 EGTA, 2 MgATP and 0.3 NaGTP (pH 7.3, 280 mOsm). mPFC pyramidal cells were identified based on their shape and prominent apical dendrite at 40x magnification under infrared and diffusion interference contrast microscopy using an inverted Olympus BX51W1 microscope (Olympus America, Center Valley, PA, USA) coupled to a Hamamatsu C8484 camera (Hamamatsu, Middlesex, NJ, USA). mPFC recordings were made in voltage clamp at a holding potential of -70 mV. Optogenetic stimulation was done with a blue LED (465 nm; PlexBright LD-1 Single Channel LED Driver from Plexon) connected via patchcords to a rotary joint that was then connected via patch cords (200 μm, 0.22 NA) to the light fiber, which was placed just adjacent to the 40x field of view. Light pulses were 5 ms long and were delivered at 8 Hz for 10 seconds. Sinusoids were generated with an Arduino device and custom-made code at 8 or 20 Hz for 10 seconds. Both signals were sent to the LED via the analog channel of the LED Driver.

Identification of EPSCs was performed using Clampfit (Molecular Devices) and MiniAnalysis (Synaptosoft, Fort Lee, NJ, USA) software. For certain experiments 20 μM CNQX and 50 μM APV (Tocris Biosciences, Avonmouth, Bristol, UK) were added to the perfusate as detailed in the manuscript.

QUANTIFICATION AND STATISTICAL ANALYSIS

Behavioral analysis

A trained observer scored time spent in the open arms and entries (4 limbs inside open arms) across light periods. For the 8- and 20-Hz behavioral experiments the trained observer was blinded. For the calculation of % open entries, the number of open arm entries was divided by the total number of entries (both open and closed arms). If a given animal did not make any entries in a light epoch, we reported 0% open entries. For EPM compartment analyses in Figures S1 and S2, the EPM data were separated based on the maze compartment (open arms, closed arms or center) in which each mouse was located when every light onset occurred. Since there are two light epochs per mouse each animal contributed two pairs of data points. Each ON epoch was paired with the OFF epoch that preceded it to be plotted. Distance traveled for mice implanted with electrodes was calculated by tracking a small LED in the headstage of mice with Neuralynx software and for mice implanted with fibers only by tracking the animal body with idTracker software (Pérez-Escudero et al., 2014). For calculating the open arm probability (Figure 6E) a vector of 120 bins was generated for both light ON epochs per mouse (each bin represented a second out of 120 s of the epoch duration) and it contained zeros or ones indicating the absence or presence, respectively, of the mouse in open arms. Then the vectors were averaged across mice, such that an average of 0 indicates that no mice were in the open arms in that second and an average of 1 indicates that all mice were in the open arms in that second. Distance traveled was calculated for periods when the mice were in the closed arms during light off and light on epochs correcting for jitter of the tracking system, and they were reported using arbitrary units. Data from light off and on periods were averaged per animal and separated by stimulation epoch where shown. Statistical comparisons were made within mice across light on and off conditions with paired t-tests used to compare behavior during light off and on periods (when pooled across stimulation epochs). 2-way repeated measures ANOVAs, with factors of light (off and on) and stimulation epoch (one and two), and Bonferroni's post hoc tests corrected for multiple comparisons were used to compare behavior across the four distinct test phases. All plots reflect group means and error bars reflect standard errors.

In vivo electrophysiology

All statistical comparisons for *in vivo* data were done with non-parametric paired (sign-rank) or unpaired (rank-sum) Wilcoxon tests. All firing rate bar plots reflect group mean and error bars reflect standard error. Phase locking to the optical stimulus was calculated using the phase component of a Hilbert transform of the recorded Arduino signal. The peak of the optical sinusoid and the center of the optical pulse corresponded to phase zero in phase locking analyses. A given unit was said to be significantly phase-locked if the distribution of the optical phases where the spikes occurred was not uniform as assessed with Rayleigh's test for non-uniformity of circular data also known as the circular r test. Zero phase corresponds to the peak of the signal. Phase locking strength was quantified using pairwise phase consistency (PPC) which is not normally distributed, therefore non-parametric statistics were used where relevant (Vinck et al., 2010). Coherence between the optical stimulus and the vHPC LFP was calculated with the two light ON epochs concatenated and using magnitude-square coherence (mscohere) Matlab function (Mathworks, Natick, MA, USA) using a window size of 1 second with 90% overlap. For the coherence over time analysis, we used the same window size and overlap for the function and calculated the average coherence for 10 seconds at a time.

Ex vivo electrophysiology

Event frequencies were calculated by dividing the total number of events by the total time in which they were recorded or in 1 second bins for Figure 2D. The frequency and amplitude of EPSCs were compared within cells at baseline and during optical stimulation in Prism (GraphPad Software, La Jolla, CA) using a repeated-measures two-way ANOVA, followed by Bonferroni post-hoc comparisons, where necessary. Phase locking of EPSCs to the light stimulation was calculated in Matlab. The degree of phase-locking of EPSCs to the optical stimulus was analyzed in Matlab using the Wilcoxon rank-sum test; the percent of cells significantly phase-locked to the optical stimulus was analyzed in Matlab using a Chi-square.

DATA AND CODE AVAILABILITY

The data and custom code supporting the current study can be made available from the corresponding author on request.